Original Article

Liquid-phase flash sintering 8YSZ with alkali halide sintering aids

J.C.C.A. Diaz*, R. Muccillo

Center of Science and Technology of Materials, Energy and Nuclear Research Institute, Travessa R 400, Cidade Universitária, S. Paulo, SP 05508-170, Brazil

ABSTRACT

The properties of ZrO_2: 8 mol% Y_2O_3 (8YSZ) ceramics with LiF and KCl sintering aids for liquid phase formation during electric field-assisted sintering were studied. Sintering experiments were carried out at 650 °C under 200 V cm^{-1} AC electric field by varying current density, current application time, as well as LiF and KCl contents. Pellets sintered with KCl addition had cavities, cracks and fractures. Pellets sintered with 15 wt.% LiF, on the other hand, were homogeneous after thermal removal of LiF upon Joule heating. Low electric current densities coupled with longer application times produced homogeneous specimens. Three different stages were identified during sintering experiments: (i) LiF melting with the electric field applied at furnace temperatures lower than its melting point, (ii) shrinkage due to liquid phase formation and LiF removal, (iii) final densification due to grain growth and pore elimination. The electrical behavior and an estimate of the porosity were carried out by electrochemical impedance spectroscopy measurements.

1. Introduction

Sintering is evidenced from the bonding and diffusion between the contacting particles during thermal treatment, resulting in a reduction of surface area and consequent densification of the sample. Pore structure and compact properties depends directly on the rate of interparticle bonding during sintering. During liquid-phase sintering a liquid phase coexists with a solid particulate at the sintering temperature. The liquid phase enhances atomic diffusion with respect to the concurrent solid state processes. The liquid can result from melting of one component, furthermore, the liquid may be transient or persistent during sintering [1,2].

Electric field assisted sintering (EFAS) techniques represent promising methods for reducing temperature and sintering time of ceramic materials. Particularly, there is a current interest in pressureless electric field assisted sintering, originally named flash sintering, as a rapid sintering method, that permit synthesis and sintering of ceramics and prevent practical problems like volatilization and high sintering temperatures [3–7]. During flash sintering experiments, densification via liquid formation or defects chemistry modification can be promoted by using selected sintering aids [8,9].

Flash sintering is based on applying an electric field (AC or DC) across a ceramic compact during thermal treatment. The flash sintering process is usually divided into three stages: the first one is the incubation, the current density being usually too low to cause significant sintering and the system working under voltage control; the second

stage, where the flash event takes place, is characterized by the switch from voltage to current control, where most of the densification takes place, with modest grain growth; the third stage is the steady stage, when the electrical parameters and power dissipation are stabilized, residual densification occurs and grain growth can happen.

Some mechanisms were proposed as responsible for the enhanced diffusion during the flash event: rapid heating due Joule effect, resulting in destabilization of the grain boundaries [10,11]; creation and migration of Frenkel pairs induced by the electric field [10,12]; and local melting or softening of the particle surfaces due to inhomogeneous temperature distribution [13–15]. Very recently, an unified model that contemplates all these mechanisms was proposed [16].

During flash sintering experiments the action of local melting or softening can be magnified using compounds that become liquid, and the combined effect of electric field induced softening at the grain boundaries and liquid-phase sintering can be evaluated.

In this work, sintering aids were used to induce a transient liquid phase during flash sintering experiments. The involved mechanisms during pressureless electric field-assisted sintering of 8YSZ using alkali halide sintering aids (KCl and LiF) as liquid phase formers were analyzed.

2. Experimental

ZrO_2: 8 mol% Y_2O_3 ceramic powders (8YSZ, tape cast grade powder, Fuel Cell Materials, USA) were dry mixed with different contents of KCl

---

* Corresponding author.
E-mail address: julio.diaz@ipen.br (J.C.C.A. Diaz).

(99.5%, Merck) and LiF (99.5%, Oregon Labware), uniaxially pressed (50 MPa) into disc-shaped pellets with 5 mm diameter and approximately 3 mm thickness, followed by isostatic pressing (140 MPa). KCl and LiF additions were in the 2–15 wt.% (5–35 vol.%) range.

A homemade experimental setup for electric field assisted sintering was used [17]. The sample was inserted in the center of a vertical furnace between two Pt disks connected via Pt wires to an AC power supply (Pacific Power Source 118-ACX, Irvine, CA, USA). Sample thickness was monitored with a computer controlled micrometric dial gauge and sample temperature with a chromel-alumel thermocouple with its tip located close to the sample.

Two sintering experiments were performed: (1) dynamic, by applying 200 V cm^{-1} AC field to the sample during furnace heating at 5 °C min^{-1} from room temperature up to the occurrence of an increase of the electric current through the sample (electric current percolation event); (2) isothermal, applying the same electric field when the sample reached 650 °C (temperature that occurred the electric current percolation event in the dynamic experiment). The power supply was set to switch to current control when the current density reached a preset value, between 25 mA mm^{-2} and 100 mA mm^{-2} (0.5 A to 2.0 A). For comparison purpose, some samples were conventionally sintered at 1400 °C for 2 h. The residual porosity of the sintered samples was evaluated using the hydrostatic Archimedes technique.

The morphological and microstructural characteristics were observed on surfaces of the sintered samples in a scanning electron microscope (Inspect F50 FEG-SEM, FEI, Brno, Czech Republic).

Impedance spectroscopy measurements were carried out in samples with silver paste on both parallel surfaces from 5 Hz to 13 MHz, 200 mV input signal, at temperatures between 270 °C and 490 °C, with an impedance analyzer (Hewlett Packard 4192A, Yokokawa, Japan) connected to a controller (Hewlett Packard 360, USA).

3. Results and discussion

Dynamic electric field-assisted sintered 8YSZ with additions of either KCl or LiF produced similar results, with the electric current percolation event occurring at 650 °C, that temperature being then set for the isothermal experiments. It is noteworthy that the electric current percolation event occurred at furnace temperatures below the melting point of the sintering aids (KCl ~772 °C, LiF ~842 °C).

Isothermal sintering experiments with application of an AC electric field were performed for different values of electric current density, current application time and alkali halide contents. Sample shrinkage and temperature were monitored during the experiments.

Samples sintered with KCl additions produced voids, cracks, and fractures (Fig. 1a), being discarded. Samples with LiF, on the other hand, had defects on the outer surfaces, being then removed by polishing, becoming homogeneous and easy to handle. At microscopic level, SEM images show rounded contours and non-polygonal grains, indicating the occurrence and effect of liquid phase during sintering with KCl and LiF additions, Figs. 1b and 2 respectively. These figures show the evolution of the microstructure of the samples with the increase of the electric current.

The achieved sample linear shrinkage level was in the 5–15% range, depending on electric current and elapsed time under electric current. As the thermocouple tip was located near but not in contact with the sample, the monitored temperature shows the relative thermal variations at the sample. Fig. 3 shows electric power, thickness shrinkage and temperature (near the sample) of 8YSZ-15 wt.% LiF as a function of time during application of 200 V cm^{-1}, limiting the value of the electric current to 1.0 A. This behavior was similar in all experiments with LiF as sintering aid, meaning that the differences depend mainly on the electric current elapsed time.

A similar isothermal electric field-assisted sintering experiment was carried out at 650 °C in a 8YSZ green pellet without sintering aid. There was no electric current percolation event, a confirmation of the role of

LiF as sintering aid responsible for the electric current percolation event with densification of 8YSZ.

In Fig. 3, region a, the observed increase of the electric power, without any change in the sample thickness, may be an indication that during this time interval LiF reached the melting point. The LiF liquid phase then disperses and impregnates the empty spaces, resulting in the observed shrinkage (Fig. 3, region b); at this stage, LiF is expected to be at least partially thermally removed from the sample. In regions b and c no significant temperature (near the sample) variation was observed, however, one should consider that the shrinkage behavior is dependent on Joule heating, by its turn, depends on the electric current produced by the application of the AC electric voltage. An estimate of the sample temperature T (during the electric current flow through the sample) was done taking into account the black body radiation model [10,12]: $T = [T_0^4 + W/A \cdot \sigma]^{1/4}$, T_0, W, A and σ stand for the furnace temperature (K), the electric power (W) dissipated in the sample, the exposed surface area of the sample (m^2) and the Stefan–Boltzmann constant 5.67×10^{-8} W m^{-2} K^{-4}, respectively. Fig. 4 presents the estimated temperatures for a representative set of sintered samples.

The evaluated temperatures are similar to the conventional sintering temperatures for 8YSZ, meaning that the sample during the electric field-assisted sintering experiments reached a temperature high enough to thermally remove the sintering aid (0.04–0.67 atm is the LiF vapor pressure at the evaluated temperatures [18]), additional removal of molten LiF by capillary action and fluidity may be expected [14]. After removal, the electric current continued to flow through the 8YSZ sample, leading to a new shrinkage process, as evidenced by region c of Fig. 3.

In summary, the electric field applied at furnace temperatures lower than the melting point of the sintering aids was able to induce a current flow through them; the heating of the sample due to the Joule effect induced the formation of a liquid phase that impregnated the empty spaces and enhanced the rate of interparticle bonding, promoting neck formation; the sample temperature increased to temperatures higher than 1250 °C (depending on the value set for the maximum electric current); the current flow remained after the thermal removal of the sintering aid, allowing for a final densification due to grain growth in the established skeletal structure. This sintering process allows then to control the densification of the samples in the 60–75% range, with electric currents between 0.5 A and 2.0 A and current application time between 20 min and 120 min.

In the present results, the observed stages during the electric field assisted sintering experiments were essentially different from those observed in Flash Sintering. The incubation time is very short or absent; here, the electric current percolation event was characterized by the switch from voltage to current control (similar to the flash event) but without densification; instead, liquid phase formation took place and the condition for an initial liquid-phase sintering was established (region a of Fig. 3); the steady stage (unlike what is expected in flash sintering) was not fully reached. The changes in the electrical parameters and power dissipation happen because at this stage densification took place, first by liquid-phase sintering (region b of Fig. 3) and then by grain growth due to the persistent electric current flow (region c of Fig. 3).

Considering the labeling of Fig. 4, hereinafter the samples will be named as indicated in Table 1.

Impedance spectroscopy data were collected from 490 °C down to 270 °C at ~25 °C steps. The impedance spectroscopy plots of the Sample 2 (see Table 1) at different temperatures are presented in Fig. 5. These plots are composed of two partially overlapped semicircles due to the contribution of grains (high frequency region) and grain boundaries (low frequency region).

Grain and grain boundary contributions were fitted according to an equivalent circuit composed of two R∥CPE elements. Depressed semicircles were observed due to the distribution of grain sizes and porosity. Each semicircle corresponds to the parallel combination of a resistance
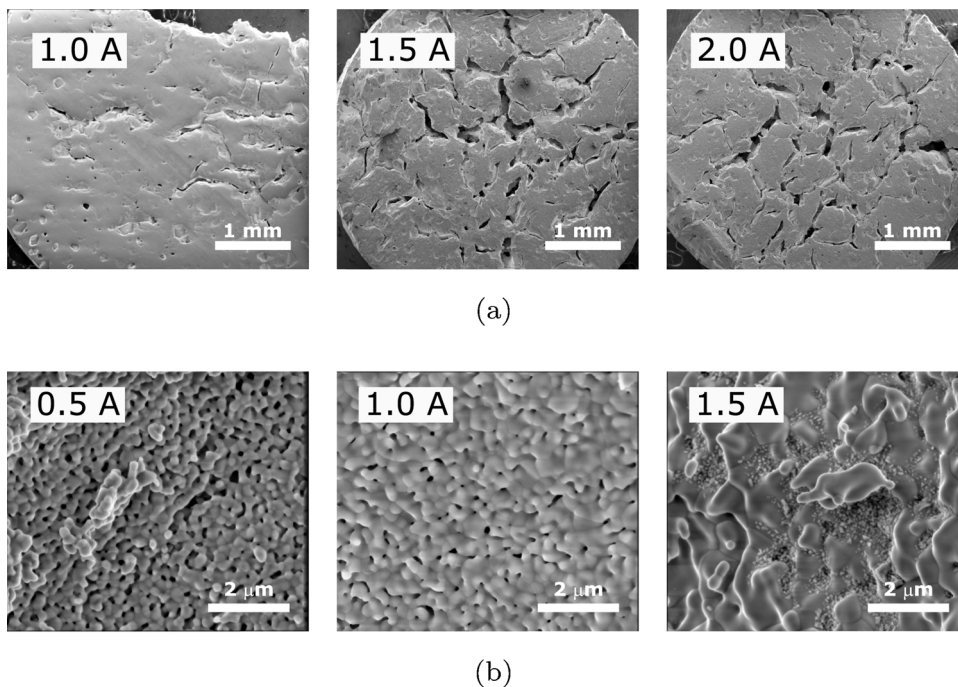
Fig. 1. SEM micrographs of 8YSZ-10 wt.% KCl sintered with application of electric field during 5 min. (a) low magnification images showing large voids, cracks and fractures; (b) high magnification images showing increasing submicron grain sizes for increasing limit of the electric current.
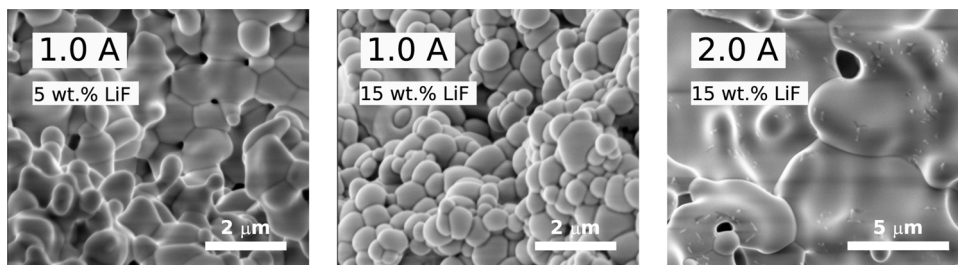

Fig. 2. SEM micrographs of 8YSZ-5 wt.% LiF and 8YSZ-15 wt.% LiF sintered with application of electric field during 20 min. Grain growth is apparent for increasing limit of the electric current.
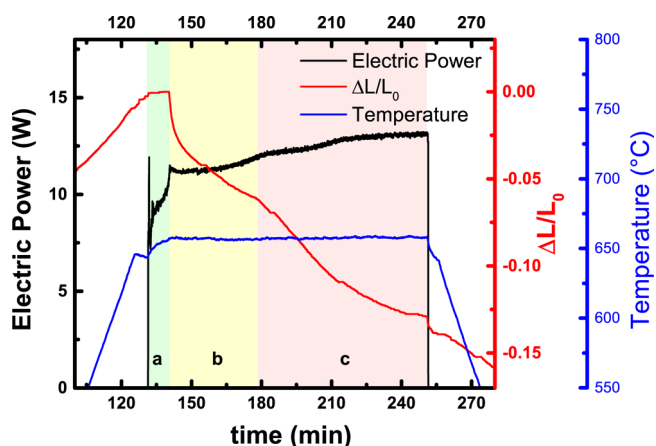

Fig. 3. Electric power, thickness shrinkage and temperature (near the sample) as a function of time in 8YSZ-15 wt.% LiF under application of $200\,V\,cm^{-1}$ limiting the electric current to 1.0 A.

Fig. 4. Evaluated temperature achieved by four electric field-assisted sintered 8YSZ-LiF samples according to the black body radiation model (see text for details), the temperature for conventional sintering of 8YSZ was also included.

$$Z \simeq \left(\frac{1}{R_g} + \frac{1}{Z_{CPE_g}} \right)^{-1} + \left(\frac{1}{R_{gb}} + \frac{1}{Z_{CPE_{gb}}} \right)^{-1}$$

and a constant phase element (CPE). The impedance of CPE is: $Z_{CPE} = (Q \cdot (i\omega)^n)^{-1}$, where $\omega = 2\pi \cdot f$, f is the excitation frequency and $\alpha = \pi/2(1 - n)$ is the decentralization angle. The impedance of the circuit was calculated according to the following expression:
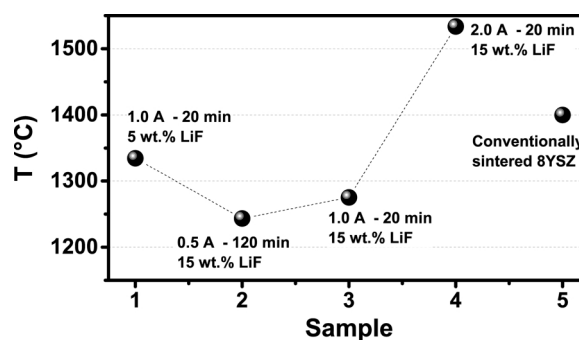
All impedance spectroscopy plots were analyzed using EIS Spectrum Analyzer software [19]. All fitted curves at each temperature showed good agreement with the experimental data. Fig. 6 shows the experimental and fitted data using the equivalent circuit at 460 °C for the same representative set of sintered samples (1 to 5) used in Fig. 4.

Table 1
Sample designation and sintering parameters.

	Sample	Sintering parameters		
		Green composition	Electric current (A)	Elapsed time (min)
EFAS, $200\,V\,cm^{-1}$, $650\,°C$	1	8YSZ-5 wt.% LiF	1.0	20
	2	8YSZ-15 wt.% LiF	0.5	120
	3	8YSZ-15 wt.% LiF	1.0	20
	4	8YSZ-15 wt.% LiF	2.0	20
		Green composition	Temperature (°C)	time (min)
Conventional sintering	5	8YSZ	1400	120
	6	8YSZ-2 wt.% KCl	1400	120
	7	8YSZ-15 wt.% LiF	1400	120

Fig. 7. Arrhenius plots of the intragranular (bottom) and intergranular (top) electrical resistivity. Results for conventionally sintered 8YSZ, 8YSZ-2 wt.% KCl and 8YSZ-15 wt.% LiF (Samples 5, 6 and 7 respectively) were included.
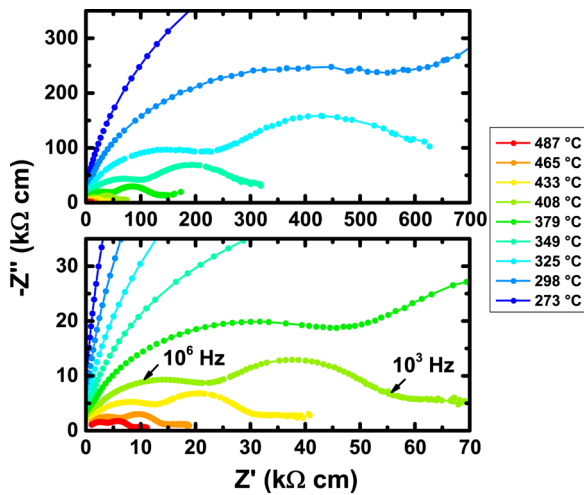

Fig. 5. Impedance diagrams at several temperatures in the 270-490 °C range of 8YSZ-15 wt.% LiF sintered with application of $200\,V\,cm^{-1}$ during 120 min, limiting the electric current to 0.5 A (Sample 2).

Fig. 8. Blocking factor times frequency factor ($\alpha_R \cdot \alpha_f$) and apparent porosity of different samples (see text for details).

As expected, the resistivity (ρ) follows an Arrhenius behavior. Fig. 7 shows the Arrhenius plots of the electrical resistivity of grains and grain boundaries; for comparison purpose, data of conventionally sintered samples were included (Samples 5, 6 and 7). The activation energies for the intragranular and intergranular thermally activated oxygen vacancies migration processes were determined as 1.0 eV and 1.1 eV respectively, in agreement with reported values for single crystals or ceramic samples with similar compositions [20,21].

In Fig. 7 no changes in the slope of the fitted straight lines were observed. A single activation energy was defined and therefore a single conduction mechanism occurred via oxide ion vacancy. As expected,
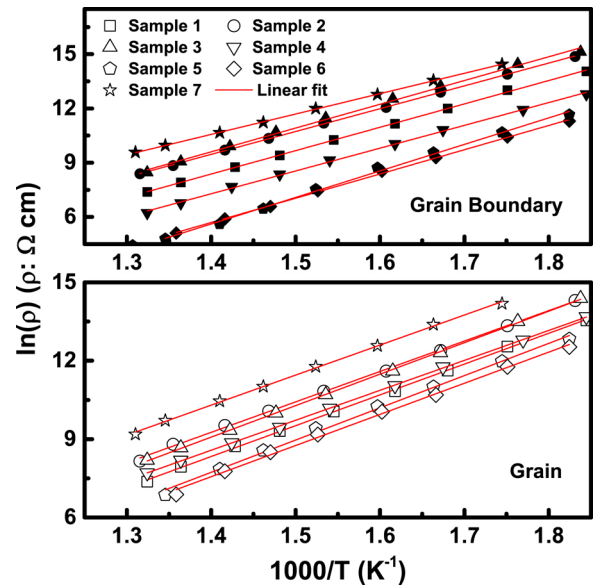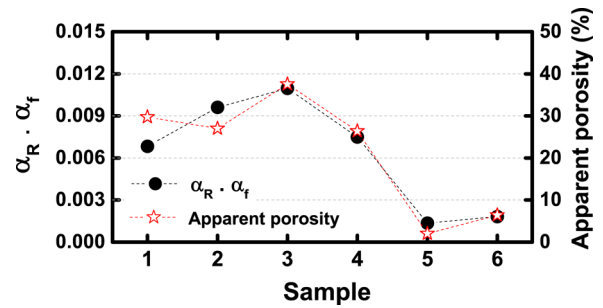
due to blocking of oxide ions at the intergranular region, the grain boundary activation energy is slightly higher than that of the bulk.

The ion blocking could be characterized by the blocking factor $\alpha_R = R_g/(R_g + R_{gb})$, and the frequency factor, $\alpha_f = f_{gb}/f_g$ [22,23]; R, f, gb, g are electrical resistance, frequency at the maximum of the semicircle, grain boundary and grain, respectively. These factors may be correlated to size parameters of the microstructure defects: α_R is proportional to the average blocking surface area and α_f to the average blocker thickness, their product ($\alpha_R \cdot \alpha_f$) is proportional to the blocker
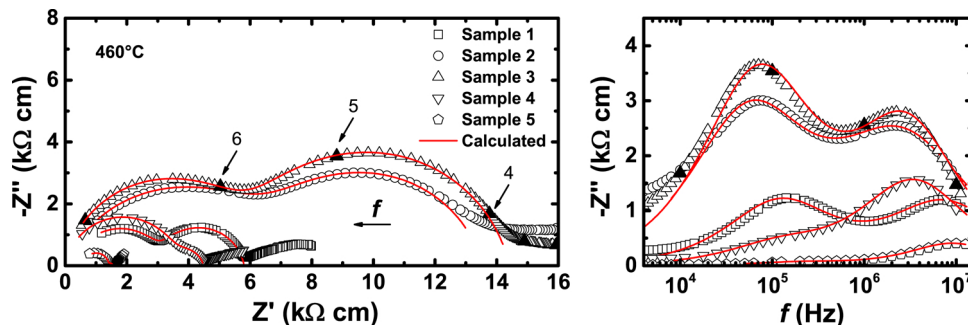

Fig. 6. Experimental and calculated impedance diagrams (left) and Bode diagrams (right) of the samples 1 to 5, measured at 460 °C. The numbers on the left side stand for log$f$ (f: Hz).

volume [23], consisting on the intergranular region associated to the porosity. For each sample $\alpha_R \cdot \alpha_f$ was evaluated in each measurement temperature and for comparison purposes the average of the values obtained is shown. Fig. 8 shows the $\alpha_R \cdot \alpha_f$ (appropriately scaled) and the apparent porosity estimated by the Archimedes method. A direct correspondence between $\alpha_R \cdot \alpha_f$ and the apparent porosity was observed, making possible to estimate a proportionality factor between them: Apparent porosity (%) $\approx (10^4/3)(\alpha_R \cdot \alpha_f)$.

From Figs. 7 and 8 one can state that the parameters during the electric field assisted sintering experiments (electric current density, current application time and sintering aid content) may be related to electrical and microstructural properties. Variations in the electric current density and current elapsed time allowed to obtain different pore contents.

4. Conclusions

Experiments on electric field-assisted sintering of ZrO_2:8 mol% Y_2O_3 (8YSZ) with additions of KCl and LiF were carried out looking for the possibility of simultaneous liquid-phase sintering at furnace temperatures below the melting point of the sintering aids, provided by Joule heating. Electric current density and time elapsed under the electric field, as well as LiF and KCl contents were the main parameters. KCl sintering aid was found to produce voids, cracks and fractures. LiF ($\sim$35 vol.%), on the other hand, was found to produce homogeneous 8YSZ specimens after its thermal removal upon Joule heating. The average grain size increased for increasing electric current limit. Low electric current density coupled to longer time under the electric field was found to produce homogeneous specimens. Formation of liquid phase due to Joule heating was considered as responsible for liquid-phase sintering and removal of LiF. The different stages during the sintering experiments were described and analyzed, differences with normal flash sintering stages were appointed. Impedance spectroscopy measurements at several temperatures allowed for evaluating the activation energies from the Arrhenius plots, as well as an estimate of the relative pore content using the blocking and frequency factors.

Funding

Conflicts of interest

The authors declare no conflicts of interest.

Acknowledgements

References

[1] R.M. German, Liquid Phase Sintering, Springer, Boston, MA, 1985, https://doi.org/10.1007/978-1-4899-3599-1.
[2] R.M. German, P. Suri, S.J. Park, Review: liquid phase sintering, J. Mater. Sci. 44 (1) (2009) 1–39, https://doi.org/10.1007/s10853-008-3008-0.
[3] D. Yang, R. Raj, H. Conrad, Enhanced sintering rate of zirconia (3Y-TZP) through the effect of a weak dc electric field on grain growth, J. Am. Ceram. Soc. 93 (10) (2010) 2935–2937, https://doi.org/10.1111/j. 1551-2916.2010.03905.x.
[4] R. Muccillo, M. Kleitz, E.N.S. Muccillo, Flash grain welding in yttria stabilized zirconia, J. Eur. Ceram. Soc. 31 (8) (2011) 1517–1521, https://doi.org/10.1016/j.jeurceramsoc.2011.02.030.
[5] S. Grasso, Y. Sakka, N. Rendtorff, C. Hu, G. Maizza, H. Borodianska, O. Vasylkiv, Modeling of the temperature distribution of flash sintered zirconia, J. Ceram. Soc. Jpn. 119 (2011) 144–146, https://doi.org/10.2109/jcersj2.119.144.
[6] M. Biesuz, V.M. Sglavo, Liquid phase flash sintering in magnesia silicate glass-containing alumina, J. Eur. Ceram. Soc. 37 (2) (2017) 705–713, https://doi.org/10.1016/j.jeurceramsoc.2016.08.036.
[7] L.M. Jesus, R.S. Silva, J.-C. M'Peko, Ultrafast synthesis and sintering of materials in a single running experiment approach by using electric fields, J. Adv. Ceram. 8 (2) (2019), https://doi.org/10.1007/s40145-018-0313-1.
[8] V.M. Candelario, R. Moreno, R.I. Todd, A.L. Ortiz, Liquid-phase assisted flash sintering of SiC from powder mixtures prepared by aqueous colloidal processing, J. Eur. Ceram. Soc. 37 (2) (2017) 485–498, https://doi.org/10.1016/j.jeurceramsoc.2016.08.024.
[9] R. Muccillo, A.S. Ferlauto, E.N.S. Muccillo, Flash sintering samaria-doped ceria – carbon nanotube composites, Ceramics 2 (1) (2019) 64–73, https://doi.org/10.3390/ceramics2010006.
[10] R. Raj, Joule heating during flash-sintering, J. Eur. Ceram. Soc. 32 (10) (2012) 2293–2301, https://doi.org/10.1016/j.jeurceramsoc.2012.02.030.
[11] Y. Zhang, J. Nie, J.M. Chan, J. Luo, Probing the densification mechanisms during flash sintering of ZnO, Acta Mater. 125 (2017) 465–475, https://doi.org/10.1016/j.actamat.2016.12.015.
[12] M. Cologna, B. Rashkova, R. Raj, Flash sintering of nanograin zirconia in < 5 s at 850 °C, J. Am. Ceram. Soc. 93 (11) (2010) 3556–3559, https://doi.org/10.1111/j.1551-2916.2010.04089.x.
[13] J. Narayan, A new mechanism for field-assisted processing and flash sintering of materials, Scr. Mater. 69 (2) (2013) 107–111, https://doi.org/10.1016/j.scriptamat.2013.02.020.
[14] R. Chaim, Liquid film capillary mechanism for densification of ceramic powders during flash sintering, Materials 9 (4) (2016) 280, https://doi.org/10.3390/ma9040280.
[15] R. Chaim, Particle surface softening as universal behaviour during flash sintering of oxide nano-powders, Materials 10 (2) (2017) 179, https://doi.org/10.3390/ma10020179.
[16] J. Narayan, Unified model of field assisted sintering and related phenomena, Scr. Mater. 176 (2020) 117–121, https://doi.org/10.1016/j.scriptamat.2019.09.012.
[17] S.G.M. Carvalho, Contribution to the Study of Electric Field-Assisted Pressureless Sintering Tetragonal Yttria-Stabilized Zirconia, University of S. Paulo, Brazil, 2018, https://doi.org/10.11606/T.85.2018.tde-11042018-081349 Doctoral Thesis.
[18] D.L. Hildenbrand, W.F. Hall, F. Ju, N.D. Potter, Vapor pressures and vapor thermodynamic properties of some lithium and magnesium halides, J. Chem. Phys. 40 (10) (1964) 2882–2890, https://doi.org/10.1063/1.1724921.
[19] A.S. Bondarenko, G.A. Ragoisha, Progress in Chemometrics Research, Nova Science Publishers, New York, 2005, pp. 89–102.
[20] A. Rivera, J. Santamaría, C. Leon, Electrical conductivity relaxation in thin-film yttria-stabilized zirconia, Appl. Phys. Lett. 78 (5) (2001) 610–612, https://doi.org/10.1063/1.1343852.
[21] M. Weller, R. Herzog, M. Kilo, G. Borchardt, S. Weber, S. Scherrer, Oxygen mobility in yttria-doped zirconia studied by internal friction, electrical conductivity and tracer diffusion experiments, Solid State Ionics 175 (1–4) (2004) 409–413, https://doi.org/10.1016/j.ssi.2003.12.044.
[22] M. Kleitz, L. Dessemond, M. Steil, Model for ion-blocking at internal interfaces in zirconias, Solid State Ionics 75 (1995) 107–115, https://doi.org/10.1016/0167-2738(94)00143-G.
[23] M.C. Steil, F. Thevenot, M. Kleitz, Densification of yttria-stabilized zirconia impedance spectroscopy analysis, J. Electrochem. Soc. 144 (1) (1997) 390–398, https://doi.org/10.1149/1.1837416.